Journal of Power Sources 196 (2011) 4747–4755

Contents lists available at ScienceDirect

Journal of Power Sources

journal homepage: www.elsevier.com/locate/jpowsour

The doping effect on the crystal structure and electrochemical properties of $LiMn_xM_{1-x}PO_4$ (M = Mg, V, Fe, Co, Gd)

Gang Yang[a,b,*], Huan Ni[a], Haidong Liu[a], Po Gao[a], Hongmei Ji[a], Soumyajit Roy[a], João Pinto[b], Xuefan Jiang[a,**]

[a] Jiangsu Laboratory of Advanced Functional Material, School of Chemistry and Materials Engineering, Changshu Institute of Technology, Changshu 215500, China
[b] I3N, University of Aveiro, 3810-193 Aveiro, Portugal

ARTICLE INFO

Article history:
Received 16 August 2010
Received in revised form
14 December 2010
Accepted 19 January 2011
Available online 26 January 2011

Keywords:
Lithium secondary batteries
Cathode material
Doping effect
Electrochemical performance

ABSTRACT

To substitute minor Mn^{2+} by the transition metal ion M = Mg^{2+}, V^{3+}, Fe^{2+}, Co^{2+}, or Gd^{3+}, $LiMn_{0.95}M_{0.05}PO_4$ samples are synthesized by a solid-state reaction route. The interpretation of doping effects is complicated by the interrelations between doping microstructure and morphology, because the crystal structure would be affected by the doped elements. The lattice structure and deviation of Li–O bond lengths of the doped $LiMnPO_4$ are refined by XRD refinement. All the samples present a couple of oxidation and reduction peaks in cyclic voltammetry, corresponding to a redox Mn^{3+}/Mn^{2+} reaction coupled with the extraction/reinsertion process of Li^+ in $LiMnPO_4$ structure. During charge/discharge process, the electron flowing and Li^+ cation diffusion in the various doped $LiMnPO_4$ samples should be different thermodynamic and kinetic process. For further studying which step in thermodynamic and kinetic process would affect or control the electrochemical performance, the initial charge/discharge capacities and cycleability of doped $LiMnPO_4$ samples are obtained under different voltage range (from 2.7 to the upper cut-off voltage 4.4, 4.6 and 4.8 V, respectively) and different environment temperatures (0, 25, and 50 °C). At relative higher measuring temperature, the discharge capacity of Co-doped $LiMnPO_4$ shows 151.9 mAh g^{-1}.

1. Introduction

Lithium transition-metal phosphates $LiMPO_4$ (M = Mn, Fe, Co and Ni) have recently attracted much attention due to their lower toxicity, lower cost, higher electrochemical and thermal stabilities [1–3]. $LiMnPO_4$ become another very promising cathode material for lithium ion batteries beside $LiFePO_4$ [5–7]. $LiMnPO_4$ should be a more ideal substitute for $LiCoO_2$ because the working potential (about 4.1 V) is very close to that of $LiCoO_2$ [5–9]. However, poor charge/discharge capacity and cycle performance of $LiMnPO_4$ even at a reasonably low current density, have limited their practical application in high power batteries. Till date only an acceptable discharge capacity has been achieved at low current densities and under trickle charge mode tests. The poor electrochemical performance of $LiMnPO_4$ is mostly for the intrinsically low electronic conductivity and/or slow diffusion of Li-ion through $LiMnPO_4$ particles [10–12].

To overcome such short-comings of $LiMnPO_4$ in recent years, one such synthetic approach for improving the electrochemical performance of $LiMnPO_4$ is to minimize the particle size and obtain uniform particle size distribution with preferential morphology [7–9,13–18]. For instance, Wang et al. synthesized particles of $LiMnPO_4$ as small as 100 nm, and reported a reversible capacity of 70 mAh g^{-1} at 0.05*C* rate [8]. Delacourt et al. synthesized 100 nm diameter particles of $LiMnPO_4$ by precipitation method, which enhanced the reversible capacity to 70 mAh g^{-1} compared with only 35 mAh g^{-1} for 1 μm diameter particles [16]. Kwon et al. [9] reported $LiMnPO_4$ with a size of 130 nm synthesized by sol–gel route showing a reversible capacity of 134 mAh g^{-1} at 0.1*C*. Recently, Wang et al. reported platelet-like $LiMnPO_4$ with a thickness of 35 nm successfully synthesized by polyol method. The as-synthesized platelet-like $LiMnPO_4$ showed an improved reversible capacity of 159 mAh g^{-1} (*C*/10) at elevated temperature (50 °C) [7,12]. The good electrochemical performance of $LiMnPO_4$ was attributed to the constituent nanoparticle morphology since it reduced the diffusion path length for lithium ions and further created a large contact area with conductive additives such as carbon.

Carbon coating has been verified to be another efficient way which can mainly decrease the boundary resistance of crystals and thereby improve the electrochemical performance of the materials. However, minimizing the particle size and carbon coating cannot resolve the low lattice electronic conductivity or chemical diffu-

* Corresponding author at: Jiangsu Laboratory of Advanced Functional Material, School of Chemistry and Materials Engineering, Changshu Institute of Technology, Nanshanhua 99, Changshu 215500, Jiangsu, China. Tel.: +86 512 52251895; fax: +86 512 52251842.
** Corresponding author. Tel.: +86 512 52251895; fax: +86 512 52251842.
E-mail addresses: gyang@cslg.edu.cn, gangyang@ua.pt (G. Yang), xfjiang@cslg.edu.cn (X. Jiang).

0378-7753/$ – see front matter © 2011 Elsevier B.V. All rights reserved.
doi:10.1016/j.jpowsour.2011.01.064

sion ability of lithium ion within the crystal structure. The third approach involves doping transition metal cations in the lattice of $LiMnPO_4$ to improve the diffusion ability of Li^+ ions and ionic conductivity. Metal cation doped $LiMnPO_4$ is considered to reduce the availability of the Mn^{3+}/Mn^{2+} redox couple, and enhances its cathode performance [19–21]. Nie et al. showed the Jahn–Teller effects in Li_xMnPO_4 using first principles calculation. The existence of Mn^{3+} ions in Li_xMnPO_4 was further shown to be not conducive to the stability of the material during the charge/discharge process. In other words, the J–T effect induced volume and cell distortion of the electrode, would finally lead to rapid mechanical degradation of the capacity [22]. The density functional theory-based calculations on $LiMPO_4$ (M = Fe, Mn, Co, and Ni) moreover showed that the lowest Li migration energy for the nonlinear pathway along the (0 1 0) channel is a curved trajectory between Li sites. Consequently with such a one-dimensional pathway for Li migration, the lattice distortion by J–T effect in $LiMnPO_4$ might block the long-range Li conduction and thereby decrease the electrochemical performance [4].

In this work, we substitute minor Mn^{2+} by alkali-, transition-, and inner transition-metal ions, like M = Mg^{2+} (alkali metal ion), V^{3+}, Fe^{2+}, Co^{2+} (transition metal ions) and Gd^{3+} (inner-transition metal ions) to synthesize $LiMn_{0.95}M_{0.05}PO_4$ doped samples. The synthesized materials have been thoroughly characterized using XRD, cyclic voltammetry (CV), and their charging/discharging capacities have been tested at various cut-off voltages and different testing temperatures. The interpretation of doping effects, in relation to the lattice structure and the electrochemical performance are discussed in detail.

2. Experimental

2.1. Preparation of $LiMnPO_4$ and doped samples

A stoichiometric ratio of lithium acetate, manganese acetate, and citric acid are mixed and dissolved in water at room temperature. Citric acid is used here as a carbon source. The added doping precursor includes $Mg(NO_3)_2$, V_2O_5, $Co(CH_3COO)_2$, FeC_2O_4, Gd_2O_3. Aqueous $NH_4H_2PO_4$ is added into the above mixture according to the mole ratio of $LiMn_{0.95}M_{0.05}PO_4$ (M = Mg, V, Fe, Co, Gd). The mixture is stirred for 1 day and dried at 60 °C. The obtained powder is pressed into pellets at the pressure of 5 MPa, and then decomposed at 350 °C in N_2 atmosphere for 10 h. The pre-heated precursor is ball-milled for 10 h in a planetary-type ball miller, and pressed into pellets under the pressure of 5 MPa. The pellet is reacted at 700 °C for 20 h in N_2 atmosphere in a tube furnace. The obtained products have been referred to as LMMgP, LMVP, LMFeP, LMCoP, LMGdP according to the dopant $Mg(NO_3)_2$, V_2O_5, $Co(CH_3COO)_2$, $FeSO_4$, Gd_2O_3, respectively. For comparison, $LiMnPO_4$ without dopant is also prepared using the same procedure, and simply named as LMP.

2.2. Structural and morphological characterization

The crystal structure of the as-prepared samples is measured using a Rigaku diffractometer with Cu K_a radiation operating at 40 kV and 30 mA. The diffraction data are collected for 4 s at each 0.02° step width over 2θ ranging from 10 to 80°. The lattice parameters of the as-synthesized samples are refined by Rietveld analysis using the General Structure Analysis System (GSAS) [23]. The morphology is characterized using scanning electron microscope (SEM, Hitachi-X650 microscope, 20 kV). The particle size distribution is determined by the optical particle size analyzer (Mastersizer 2000, England). Elemental composition (Li:Mn) of the doped $LiMnPO_4$ samples is determined by ICP-AES (Inductively Coupled Plasma Atomic Emission Spectrometer) (Plasma-400).

2.3. Electrochemical tests

Cyclic voltammetries (CVs) are conducted on a PARSTAT2273 electrochemical workstation. In a potential range of 2.7–4.8 V (*vs* Li^+/Li), the CV profiles for the above test cells are recorded at a scan rate of 0.1 mV s^{-1} at 25 °C. A lithium foil acts as both the counter electrode and reference electrode.

Electrochemical charge–discharge performance of the samples is evaluated in model CR2016 coin cells. The as-prepared sample $LiMn_{0.95}M_{0.05}PO_4$ (M = Mg, V, Fe, Co, and Gd) is mixed with acetylene black and Teflon powder in the weight ratio 80:15:5. Lithium foil is used as the anode, and 1 M $LiPF_6$ in EC:DMC = 1:1 is used as the electrolyte. The separator is Celgard 2300 membrane. Cells are assembled in an argon-filled glove box. Cycling and charge–discharge performances of the testing cells are carried out on Land CT2001A. The cut-off voltage is controlled at the range of 2.7–4.4 V, 2.7–4.6 V, and 2.7–4.8 V *vs* Li/Li^+, respectively. The cell testing is performed under the surrounding temperature of 0, 25, and 50 °C, respectively. The temperature is controlled using Huber ministat240 (accuracy ±0.1 °C). For the entire cell testing, we adopt the constant current–constant voltage (CC–CV) in charging and constant current (CC) in discharging process. The cells are charged with a *C*/20 rate to the upper cut-off voltage, kept at the upper voltage until the *C*/100 rate, and then discharged to 2.7 V at *C*/20 = 8.5 mAh g^{-1} rate (1*C* = 170 mAh g^{-1}). The electrochemical capacity of the samples is calculated on the amount of the active material.

3. Results and discussion

Fig. 1 shows the XRD patterns of the $LiMnPO_4$ and $LiMn_{0.95}M_{0.05}PO_4$ (M = Mg, V, Fe, Co, and Gd) that are synthesized at 700 °C for 20 h in nitrogen atmosphere. All patterns are clearly indexed as orthorhombic structure of $LiMnPO_4$ with *Pnma* space group, and no other impurity phases are detected. All doped $LiMnPO_4$ samples by the various transition metal elements reveal a single-phase with a well-ordered olivine structure of $LiMnPO_4$. Compared with the detailed XRD patterns of the minor doped samples, only Fe- and Gd-doped $LiMnPO_4$ present a little shift (as shown in Fig. 1).

The scanning electron microscope (SEM) images of $LiMnPO_4$ and $LiMn_{0.95}M_{0.05}PO_4$ (M = Mg, V, Fe, Co and Gd) are shown in Fig. 2. $LiMnPO_4$ is relatively more agglomerated than the other doped samples. The Co- and Gd-doped $LiMnPO_4$ samples show relatively narrow size distribution (around 100–300 nm) of nanoparticles. All the samples present common irregular and agglomerated particles. The similarity in morphology and crystal size of all the doped samples could be indicated that there is no more effect by the doping elements, because all the doped samples are synthesized under the same reaction conditions. Fig. 3 shows the particle size distribution of doped-$LiMnPO_4$ samples. The geometric mean diameter is dependent on the minor doped transition metal elements. Most of the doped $LiMnPO_4$ samples present two part of particle size distribution, and the relatively large size might be due to the agglomerations of the nanoparticles. Compared with the geometric mean diameter of pure $LiMnPO_4$ particles, the average particle size of Fe-doped sample presents a big value, but the others present relative smaller values. The geometric mean diameter of $LiMnPO_4$, Mg, V, Fe, Co and Gd-doped samples are 397.2, 356.8, 341.2, 424.9, 305.9 and 342.8 nm. The small nanoparticle size and narrow size distribution of Co-doped $LiMnPO_4$ will be benefit for the electrochemical properties.

The XRD patterns of the doped $LiMnPO_4$ samples by various transition metal elements are refined by Rietveld analysis. The best refinement model is chosen from a *Pnma* space group. The refine-

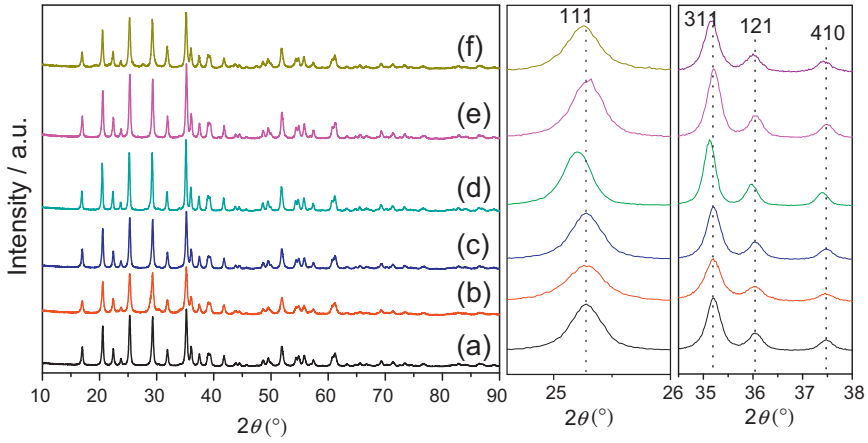

Fig. 1. XRD patterns of (a) $LiMnPO_4$, (b) Mg-doped, (c) V-doped, (d) Fe-doped, (e) Co-doped, and (f) Gd-doped $LiMnPO_4$ samples.

ments are shown in Fig. 4. The refined lattice parameters and the bond lengths are listed in Table 1. The reliability factor of $x^2 < 3$, the weighted factor R_{wp}, R_f and $R_p < 10\%$ (as shown in Table 1), show that the Rietveld refinement results obtained in the following analysis of crystal structure are reliable.

The refined cell parameters of the $LiMnPO_4$ sample are $a = 10.4357(2)$, $b = 6.0969(8)$, $c = 4.7420(9)$ Å, are consistent with the reported values in the literature [24]. Since the minor dopant element with bigger or smaller atomic radius than Mn^{2+} replaces in the lattice structure of $LiMnPO_4$, the lattice parameters of the doped samples show a little deviation compared to those of pure $LiMnPO_4$ (as shown in Table 1), even if the doping ratio is as low as 5% in mole. It implies the substituted cations enter into the lattices to form a solid solution instead of a mixture. The occupation of dopants

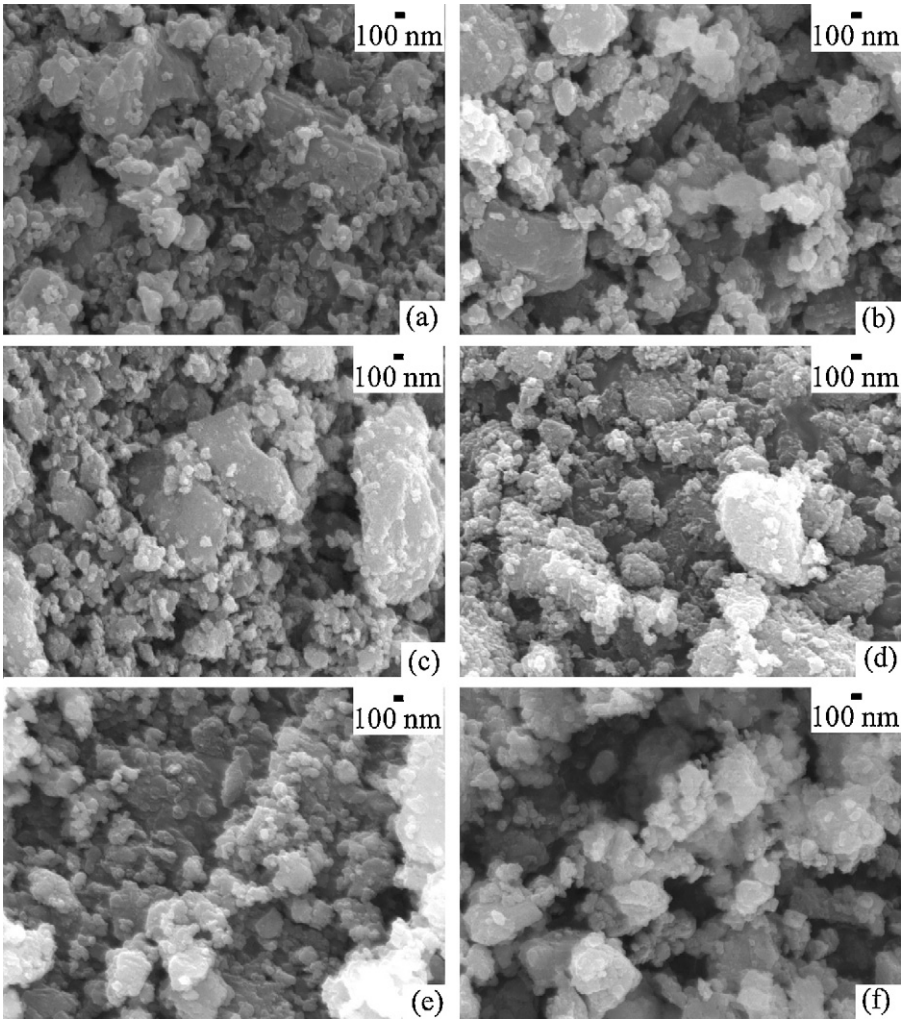

Fig. 2. SEM images of (a) $LiMnPO_4$, (b) Mg-doped, (c) V-doped, (d) Fe-doped, (e) Co-doped, and (f) Gd-doped $LiMnPO_4$ samples.

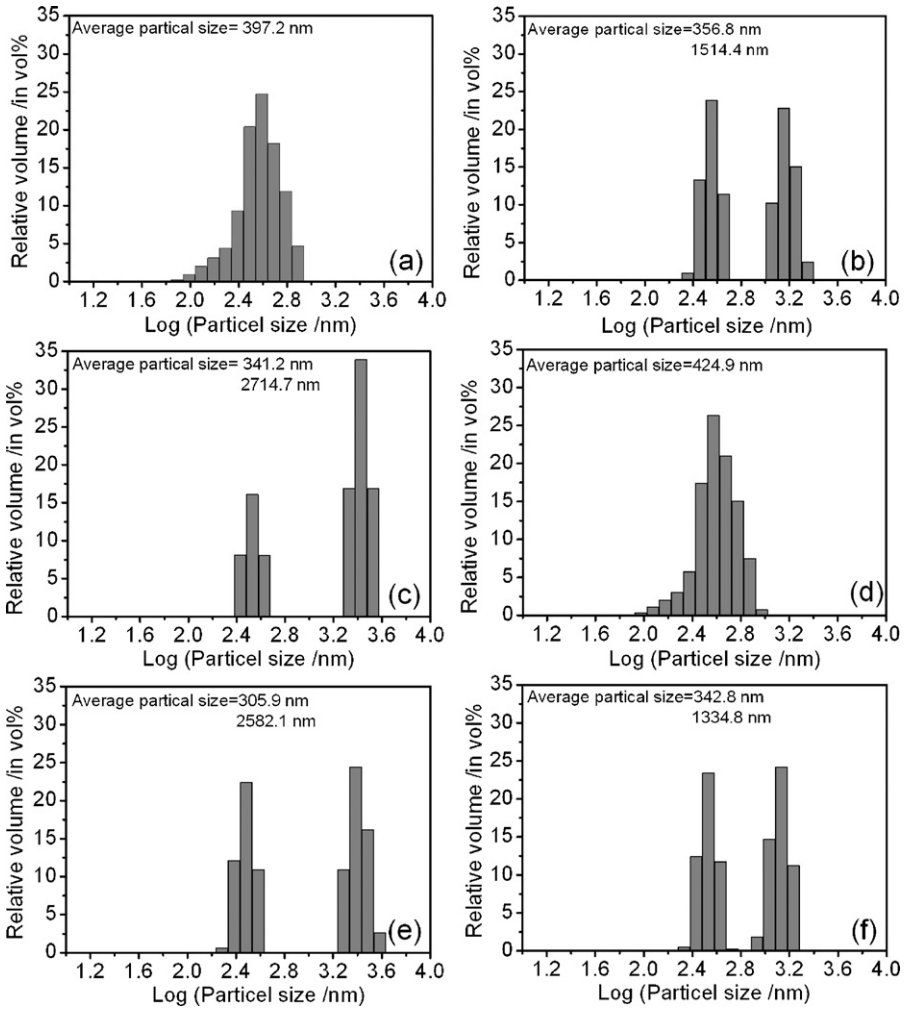

Fig. 3. Particle size distribution of (a) $LiMnPO_4$, (b) Mg-doped, (c) V-doped, (d) Fe-doped, (e) Co-doped and (f) Gd-doped $LiMnPO_4$ samples.

and vacancies in the lattice can be expected to result in very small changes of the lattice parameters [25]. Based on the ICP results, the calculated formula of the doped samples are listed in Table 1, there are deviations with the ideal value because the dopant might be locate in M1 (Li-site), M2 (Mn-site) or both, and vacancies are exist in the olivine lattice. The cell volumes present relative complex results with the ionic radii of various dopant elements, because it is hard to determine the real position M1 or M2 site of dopant located in the lattice and how many vacancies exist. Indeed the factors affecting lattice parameters remain poorly understood at present [25].

Rietveld refinement further reveals the deviation of bond length in doped crystal structure of $LiMnPO_4$ (as shown in Table 1). For a simple way, we suppose to place the doped element on M2

Table 1
Results of structure analysis calculated from XRD Rietveld refinement of $LiMnPO_4$ and $LiMn_{0.95}M_{0.05}PO_4$. Space group is *Pnma*.

Sample		LMP	LMMgP	LMVP	LMFeP	LMCoP	LMGdP
Lattice parameter (Å)	*a*	10.4357(2)	10.4483(3)	10.4501(8)	10.4296(0)	10.4566(4)	10.4487(2)
	b	6.0969(8)	6.1081(6)	6.1050(6)	6.0920(0)	6.1083(8)	6.1033(0)
	c	4.7420(9)	4.7455(4)	4.7486(7)	4.7369(8)	4.7502(4)	4.7431(9)
Lattice volume ($Å^3$)		301.7117	302.8543	302.9505	300.9690	303.4050	302.4748
Li:Mn:M		–	0.95:0.93:0.03	0.90:0.91:0.04	0.94:0.97:0.03	0.93:0.92:0.05	–
Bond lengths (Å)	Li–O1	2.2301(2)	2.2325(3)	2.2328(2)	2.2298(2)	2.2538(2)	2.2574(0)
	Li–O2	2.0823(2)	2.1254(0)	2.0833(2)	2.0960(2)	2.0920(2)	2.0894(0)
	Li–O3	2.1758(2)	2.1655(0)	2.1805(2)	2.1411(3)	2.1709(3)	2.2335(0)
	Mn–O1	2.2463(3)	2.2475(0)	2.2477(3)	2.233(4)	2.2484 (0)	2.2167(0)
	Mn–O2	2.1600(3)	2.0477(0)	2.168(4)	2.130(4)	2.1694 (0)	2.1447(0)
	Mn–O3	2.2420(2)	2.2095(0)	2.2460(2)	2.2661(3)	2.2727(3)	2.2805(0)
	Mn–O3	2.1625(2)	2.2035(0)	2.1620(2)	2.1581(3)	2.1444(2)	2.0905(0)
Reliability factors	x^2	1.58	2.37	1.68	2.62	1.48	3.02
	R_p/%	4.17	6.70	4.51	5.20	5.25	6.81
	R_{wp}/%	5.26	8.24	5.52	6.78	6.37	8.21
	R_{p2}%	2.19	5.39	2.15	3.60	2.28	7.22

M is the minor doped metal element, the ratio of Li:Mn:M are calculated based on the reference 1 of PO_4 in $Li_xMn_yM_zPO_4$ formula.

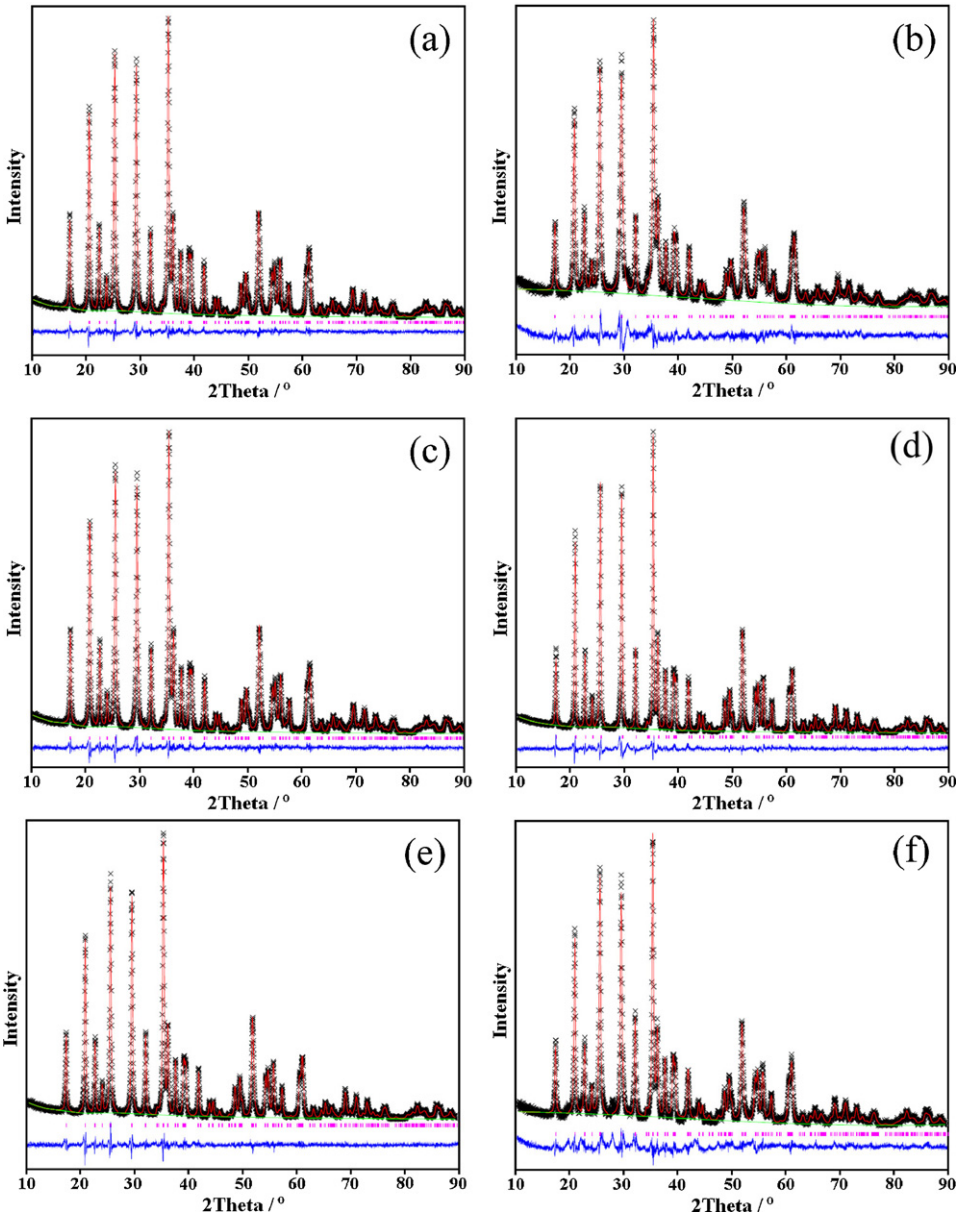

Fig. 4. Observed (×) and calculated (solid line) XRD patterns for (a) $LiMnPO_4$, (b) $LiMn_{0.95}Mg_{0.05}PO_4$, (c) $LiMn_{0.95}V_{0.05}PO_4$, (d) $LiMn_{0.95}Fe_{0.05}PO_4$, (e) $LiMn_{0.95}Co_{0.05}PO_4$, and (f) $LiMn_{0.95}Gd_{0.05}PO_4$. The difference between the observed and the calculated data is given at the bottom of the figure with the same scale. Peak positions of $LiMnPO_4$ phase are expressed as vertical lines.

(Mn-site). As well known, the diffusion ability of Li ions and the electrochemical performance of the cathode materials are always dependent on the crystal structure, such as Li–O bond lengths in the lattice. A relatively longer Li–O bond with a smaller binding energy leads to the easy migration of Li^+ cations during charge/discharge process and hence a better electrochemical performance. As shown in Table 1, there are different deviations of Li–O bond lengths of $LiMnPO_4$ samples doped by various dopant metal elements. Compared with the Li–O2 bond length 2.0823 Å in pure $LiMnPO_4$, those lengthened bonds are 2.1254, 2.0833, 2.0960, 2.0920, and 2.0894 Å in the Mg-, V-, Fe, Co, and Gd-doped samples, respectively. Moreover the Li–O bonds of Co-doped and Gd-doped $LiMnPO_4$ samples are apparently lengthened (with Li–O1 bond lengths of 2.2538 and 2.2574 Å respectively compared to that of 2.2301 Å in pure $LiMnPO_4$). The other doped samples present relatively small lengthening in Li–O1 bond lengths, except Fe-doped $LiMnPO_4$ sample. The lengthening and weakening of the Li–O bonds are expected to be conducive to enhanced electrochemical performance of cathode materials. The electrochemical performance of those doped materials with reference to above Li–O bond distances are discussed in detail in the following sections.

The CV measurements are performed on the electrode to characterize its electrochemical process of the doped materials. The second cycle of the cyclic voltammetry of $LiMnPO_4$ and doped-$LiMnPO_4$ samples is shown in Fig. 5. All the materials present a couple of oxidation and reduction peaks, corresponding to a redox Mn^{3+}/Mn^{2+} reaction coupled with the extraction and reinsertion process of the Li^+ in $LiMnPO_4$ olivine structure. The minor extra oxidation peak (near the upper cut-off potential) could be ascribed to the minor decomposition of electrolyte [8,11].

All the samples present a widened oxidation peak and relative bigger value of potential interval between the oxidation and reduction peak. It might be due to the fact that the lower conductivity limits the reversibility of Li^+ cation in olivine $LiMnPO_4$ structure. For

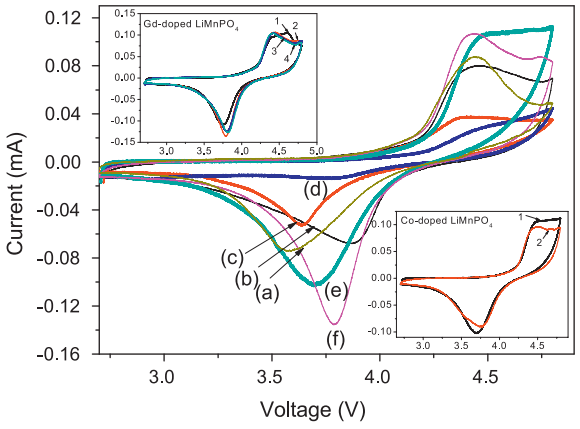

Fig. 5. Cyclic voltammetry of (a) $LiMnPO_4$, (b) Mg-doped, (c) V-doped, (d) Fe-doped, (e) Co-doped and (f) Gd-doped $LiMnPO_4$. The voltage range is 2.7–4.8 V, and the scan rate is 0.1 mV s^{-1}. The inset shows the CVs of Co-doped and Gd-doped $LiMnPO_4$ for several cycles.

example, the pure $LiMnPO_4$ sample present the biggest value 0.87 V of potential interval, but the doped-$LiMnPO_4$ samples present a relatively small potential interval between the oxidation and reduction peak. As shown in Fig. 5, the Co- and Gd-doped $LiMnPO_4$ shows strong and well-defined oxidation and reduction peaks, and the Mg-doped samples shows the narrowest potential interval between the oxidation and reduction peaks. This demonstrates the extraction/reinsertion process in the electrochemical reaction would be dependent on the dopant metal ions. The two insert images in Fig. 5 shows the overlap of the CV curves for the Co- and Gd-doped $LiMnPO_4$ samples for several cycles reflects reversibility. The Gd-doped sample demonstrates well overlap and indicates a good cycle performance.

During charge/discharge process, the electron flow and Li^+ cation diffusion in the lattice structure could be different thermodynamic and kinetic process, respectively. In general, the cut-off voltage of charge/discharge mainly affects the electron flow, and the temperature affects the diffusion of Li^+ cations. To check which step in thermodynamic and kinetic process would affect or control the electrochemical performance, the initial charge/discharge capacities and cycleability of the doped $LiMnPO_4$ samples are obtained under different voltage range (the upper cut-off voltage 4.4, 4.6 and 4.8 V, respectively) and different environment temperatures (0, 25, and 50 °C, respectively).

Fig. 6 shows the initial charge/discharge profiles and cyclic performance of the electrodes in the voltage range of 2.7–4.4 V at

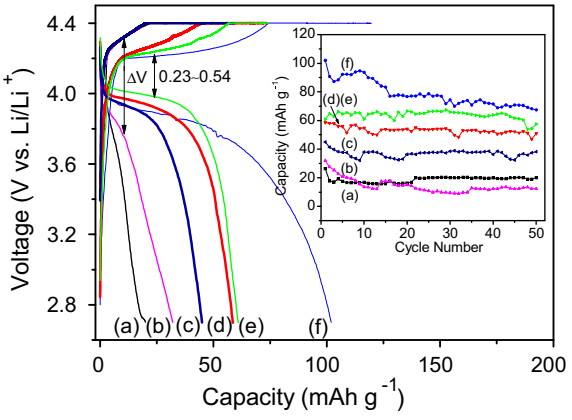

Fig. 6. Initial charge/discharge profiles and cyclic performance of (a) $LiMnPO_4$, (b) Fe-doped, (c) Mg-doped, (d) Gd-doped, (e) V-doped, and (f) Co-doped $LiMnPO_4$ samples in the voltage range of 2.7–4.4 V at 25 °C.

25 °C. As described before, many references have been reported that the electrochemical performance is always dependent on the preparation process and the obtained sample's particle morphology [6–9,14,15,26]. In this paper, irregular nanoparticles of $LiMnPO_4$ and doped-$LiMnPO_4$ samples are synthesized following the same route. Compared with the pure $LiMnPO_4$, the improved electrochemical performance of doped-$LiMnPO_4$ could be attributed to the doping effect of the minor dopant metal element in the $LiMnPO_4$ olivine structure. As shown in Fig. 6, pure $LiMnPO_4$ has less than 30 mAh g^{-1} in the initial discharge capacity, however the doped-$LiMnPO_4$ samples present big improvement in the charge/discharge capacity. It is in agreement with the above discussion of crystal structure that the lengthened Li–O bonds would increase the diffusion ability of lithium cation during charge/discharge processes. For example, at 2.7–4.4 V cut-off voltage and at 25 °C, Co-doped and V-doped $LiMnPO_4$ shows the discharge capacity of 102 and 61 mAh g^{-1}, respectively.

In the charge/discharge process of doped $LiMnPO_4$ samples (except Fe-doped sample) between the voltage 2.7 and 4.4 V, a couple of charge/discharge plateau at about 4.2/3.9 V (as shown in Fig. 6) corresponds to the compositional regions of Li_xMnPO_4, and describes the two-phase transition process in the electrochemical reaction. For different doped samples, there is 0.23–0.54 V differential between the charging and discharging voltage plateau. It indicates that there is a doping effect in the redox reaction and Li^+ diffusion ability during charging/discharging process. It quite agrees with the CV results that a couple of redox peak appeared at around 4.2/3.8 V. Moreover, all the doped $LiMnPO_4$ samples exhibited relatively well capacity retention within 50 cycles (as shown in Fig. 6).

Furthermore the doping effect should be explained that the electrochemical characteristics of the material are strongly related to their crystal structure. As discussed before, the lattice structure parameters, such as the lengthening and weakening of the Li–O bonds, are dependent on the doped transition metal elements. According to the above characterization of crystal structure and electrochemical results, the Co, V and Gd substitutions can dramatically improve the kinetic performance of $LiMnPO_4$. However, the cut-off voltage at 4.4 V is not enough to force all the lithium cations to be extracted from $LiMnPO_4$ structure. The total charge capacity is still far below the theoretical capacity of pure $LiMnPO_4$ (170 mAh g^{-1}).

The charge/discharge profiles of the doped-$LiMnPO_4$ samples at relatively high voltage (4.8 V) and high temperature (50 °C) are shown in Figs. 7 and 8, respectively. The charge capacity at CC/CV process and the discharge capacity at CC are listed in Table 2. As shown in Fig. 7, the CC discharge capacity is increased at relatively higher charge voltage 4.8 V. The doping effect is still result in different charge/discharge capacity for the doped $LiMnPO_4$ samples. For example, the Co-doped $LiMnPO_4$ presents CC charge capacity of 174 mAh g^{-1}, and the discharge capacity of 138.4 mAh g^{-1}. However, the Co-doped, V-doped $LiMnPO_4$ donot show a well cycleability, their discharge capacity show a relative loss after several cycles. It might be due to the fact that the crystal structure is unstable and the electrolyte decomposes at high voltage (4.8 V). Moreover, there is 0.32–0.84 V differential between the charging and discharging voltage plateau, bigger than those at the cut-off voltage 4.4 V (Fig. 6). It indicates that the increased cut-off voltage cannot benefit for the diffusion ability of Li^+ cations.

There have been several reports that the electrochemical performance of $LiMnPO_4$ could be improved at relatively higher testing temperature [7,18]. Using polyol synthesis method, Wang et al. synthesized nano-structured $LiMnPO_4$ with platelet morphology (about 30 nm in thickness) [7]. At elevated temperature (50 °C) this material demonstrated improved reversible capacity of 159 mAh g^{-1}. The good electrochemical performance was

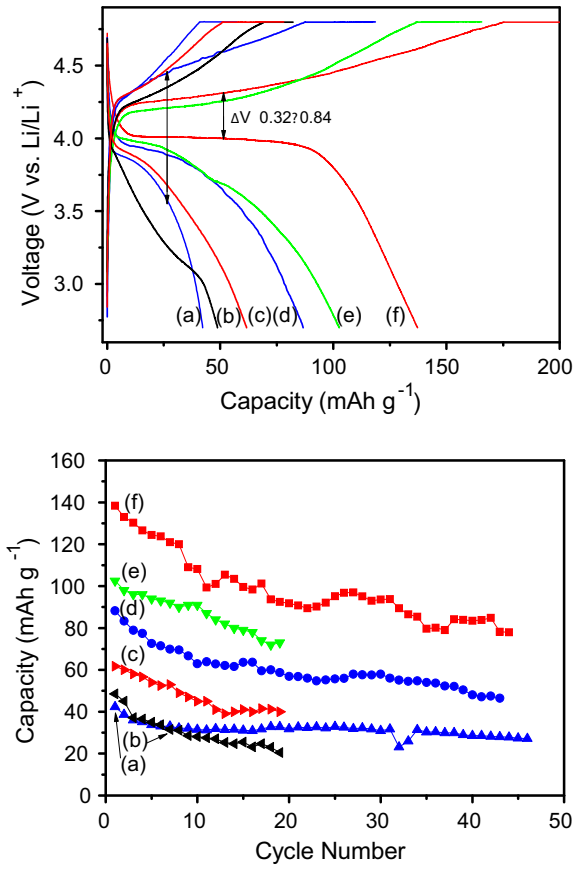

Fig. 7. Initial charge/discharge profiles and cyclic performance of (a) Gd-doped, (b) Fe-doped, (c) $LiMnPO_4$, (d) Mg-doped, (e) V-doped, and (f) Co-doped $LiMnPO_4$ samples in the voltage range of 2.7–4.8 V at 25 °C.

attributed to the well crystallized platelet shaped $LiMnPO_4$ nanoparticles oriented in the *b* direction which minimizes the paths for Li diffusion, and faster thermal motion at elevated temperature. Interestingly, the crystal morphology of doped $LiMnPO_4$ in this work consists of irregular particles without preferential orientation of lattice direction. The improved electrochemical performance could be attributed to the effect of various dopant metal ions which in turn influence the Li^+ and e^- transport in these materials rather than the constituent particle morphology.

Fig. 8 shows the charge/discharge profiles of doped-$LiMnPO_4$ under cut-off voltage 4.4 V and higher testing temperature 50 °C.

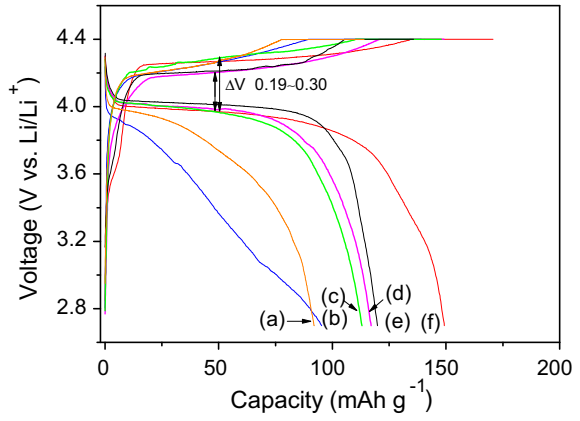

Fig. 8. Initial charge/discharge profiles of (a) $LiMnPO_4$, (b) Fe-doped, (c) Mg-doped, (d) Gd-doped, (e) V-doped, and (f) Co-doped $LiMnPO_4$ samples in the voltage range of 2.7–4.4 V at 50 °C.

Table 2
The capacities of all doped $LiMn_{0.95}M_{0.05}PO_4$ samples under different test conditions.

Test condition	Samples	Charge (mAh g^{-1})			Discharge (mAh g^{-1})
	M	CC	CV	Total	
2.7–4.4 V, 25 °C	Mg	19.9	38.8	58.7	44.9
	V	56.8	17.6	74.4	60.9
	Fe	19.3	37.0	56.3	32.0
	Co	71.0	48.6	119.6	102
	Gd	44.5	28.9	73.4	58.6
2.7–4.4 V, 50 °C	Mg	110.2	37.8	148.0	113.0
	V	105.2	30.6	135.8	119.9
	Fe	89.3	49.9	139.2	95.3
	Co	134.1	36.6	170.7	149.3
	Gd	120.5	28.6	149.1	117.0
2.7–4.8 V, 25 °C	Mg	88.2	30.4	118.6	88.2
	V	136.4	27.1	163.5	102.1
	Fe	68.1	15.2	83.3	48.5
	Co	174.0	41.3	215.3	138.4
	Gd	40.9	16.4	57.3	42.3
2.7–4.8 V, 50 °C	Co	153.5	25.0	178.5	151.9
	Gd	150.4	39.1	189.5	117.1

At relatively higher testing temperature, the doped-$LiMnPO_4$ samples show a greatly improved charge/discharge capacity. For example, the discharge capacity of Co-doped $LiMnPO_4$ reaches to 151.9 mAh g^{-1}. By comparing with the discharge capacity of doped $LiMnPO_4$ samples under higher charging voltage, the charge/discharge capacity is enhanced more by increasing the measuring temperature. The V-doped, Mg-doped and Gd-doped $LiMnPO_4$ show the discharge capacity of 119.9, 113, 117 mAh g^{-1} at cut-off voltage 4.4 V (50 °C), and 102.1, 88.2, 42.3 mAh g^{-1} at cut off voltage of 4.8 V (25 °C).

Moreover, the doped samples except Fe-doped $LiMnPO_4$ present similar discharging voltage plateau (about 3.9–4.0 V) at the cut-off voltage 4.4 V (50 °C), compared with 3.7–3.9 V of the doped samples tested at the cut-off voltage 4.8 V (25 °C). There is 0.2–0.3 V differential value between the charging and discharging voltage plateau, greatly smaller than those (0.4–0.8 V) at the cut-off voltage 4.8 V and 25 °C (Figs. 7 and 8). It indicates that the increased testing temperature can greatly benefit for the diffusion ability of Li^+ cations during charging/discharging process.

From this observation, it might be concluded that the temperature is more important than cut-off voltage for improving the electrochemical performance of $LiMnPO_4$ samples. Increasing the temperature, the diffusion ability of Li^+ cations could be increased kinetically during charge/discharge process and hence the electrochemical performance. Fig. 9 shows the charge/discharge profiles of the Co-doped $LiMnPO_4$ sample tested at 25 °C under different cut-off voltages. Along with the increasing charging voltage, the charge/discharge capacity of Co-doped $LiMnPO_4$ increased to 102.0, 114.6, and 138.4 mAh g^{-1} at the voltage 4.4, 4.6 and 4.8 V, respectively. At relatively higher cut-off voltage the discharge capacity is decreased fast after several cycles, compared with the well cycle performance occurred at 4.4 and 4.6 V. However, at the relatively higher testing temperature of 50 °C (Fig. 10) the Co-doped $LiMnPO_4$ sample shows the almost same discharge capacity, 149.3 and 151.9 mAh g^{-1} at 4.4 and 4.8 V, respectively (see also Table 2). Similar result also appears in Gd-doped sample. It further indicates that the temperature is the main factor in the electrochemical performance of olivine $LiMnPO_4$ cathode materials. Due to the doping effect, the doped $LiMnPO_4$ samples present wide range of the initial discharge capacity (from 44 mAh g^{-1} in Mg-doped $LiMnPO_4$ to 102 in Co-doped $LiMnPO_4$ shown in Fig. 6) at 25 °C, but 113 to 149 mAh g^{-1} appeared at 50 °C (Fig. 8).

Same trend is also observed in the matter of testing temperatures with the initial charge/discharge profiles of Co- and Gd-doped $LiMnPO_4$ at the same cut-off voltage (Fig. 11). It clearly shows the

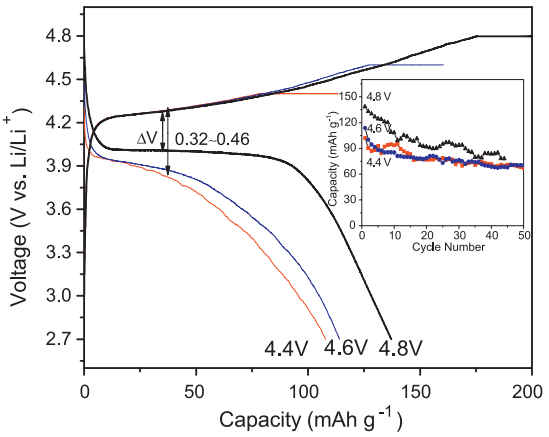

Fig. 9. Initial charge/discharge profiles of Co-doped $LiMnPO_4$ in the various cut-off voltages 4.4, 4.6, and 4.8 V, respectively. The cell is tested at the environmental temperature of 25 °C. Insert image is the cyclic performance of Co-doped $LiMnPO_4$ in the three cut-off voltage at 25 °C.

effect of temperature on the electrochemical performance of the cathode materials. At 0 °C, the Co-doped $LiMnPO_4$ shows a lowest charge/discharge capacity (less than 80 mAh g^{-1}) compared with a good discharge capacity (151.9 mAh g^{-1}) appeared at high testing temperature (50 °C). Moreover, there is a big differential plateau voltage (0.74 V) between charge and discharge process in the testing temperature at 0 °C, because there is a very low diffusion ability of Li^+ ions. The plateau appears at ca. 3.75 V in the discharge profile of Co-doped $LiMnPO_4$ at 0 °C, and at about 3.95 V at 25 °C, and 4.05 V at 50 °C, respectively. Similarly, the plateau voltage in the charge/discharge of Gd-doped $LiMnPO_4$ sample is dependent on the testing temperature. However, the Gd-doped $LiMnPO_4$ presents a relatively higher discharge capacity at 0 °C than at 25 °C. It indicates that there is a complex relation between the crystal structure of doped-$LiMnPO_4$ and the testing conditions for the best electrochemical performance due to f-shell of inner transition metal element.

Based on the above discussion, there is different electrochemical redox reaction in the doped $LiMnPO_4$ electrode processed at different cut-off voltages and test temperatures. The electron flowing and Li^+ cation diffusion in one particle of $LiMnPO_4$ sample are exist several steps and one step is the main factor to control the

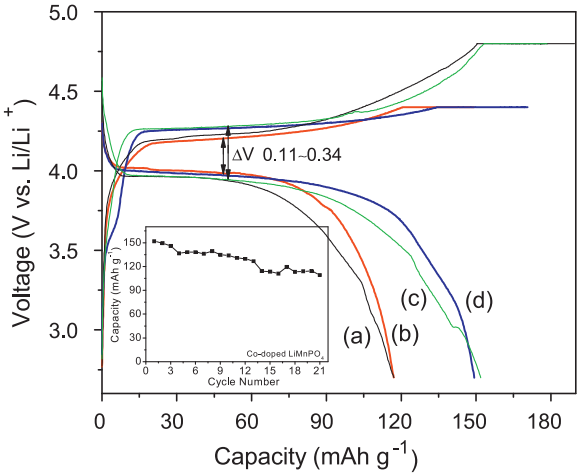

Fig. 10. Initial charge/discharge profiles of Gd-doped $LiMnPO_4$ in the voltage range (a) 2.7–4.8 V and (b) 2.7–4.4 V; and Co-doped $LiMnPO_4$ in the voltage range (c) 2.7–4.8 V and (d) 2.7–4.4 V. The cell tested at the environmental temperature of 50 °C. Insert image is the cyclic performance of Co-doped $LiMnPO_4$ in the voltage range 2.7–4.8 V at 50 °C.

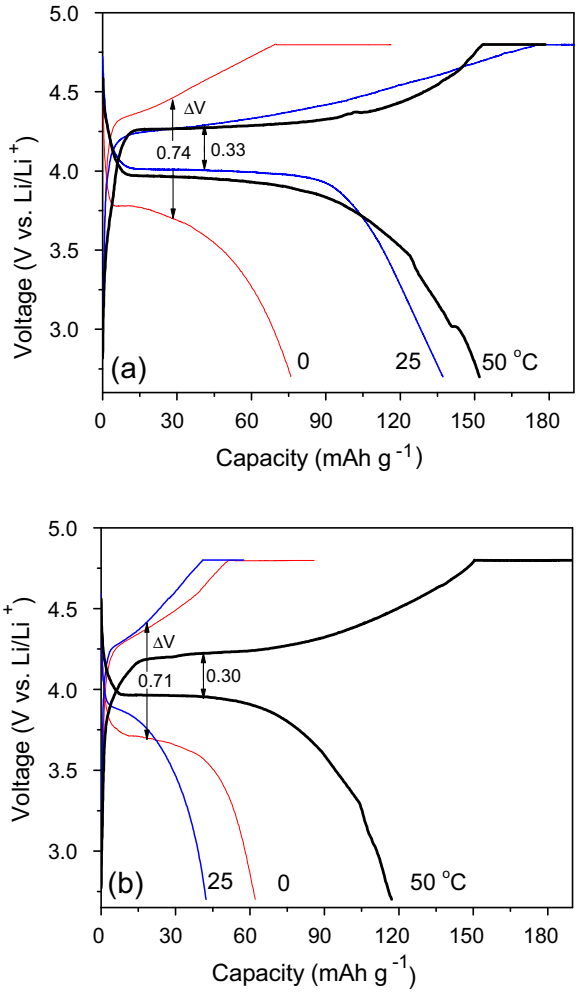

Fig. 11. Initial charge/discharge profiles of (a) Co-doped and (b) Gd-doped in the voltage range of 2.7–4.8 V at 0, 25, and 50 °C, respectively.

electrochemical properties during the electron transit and Li diffusion in a $LiMnPO_4$ particle to the collector and the electrolyte. The electron flow and Li^+ cation diffusion could be different thermodynamic and kinetic process, respectively. If we suppose the cut-off voltage of charge/discharge mainly affects the electron flow and the temperature affects the diffusion of Li^+ cations, we could here propose the redox reaction on the $LiMnPO_4$ particle in Fig. 12. During charging (oxidation) process, Li^+ cation is extracted from the lattice of $LiMnPO_4$ and transferred to the particle surface (step E1). Then Li^+ cation goes through the carbon coated on the surface of $LiMnPO_4$ particles (step E2), and diffuses into the electrolyte (step E3). At the same time, an electron also goes through the $LiMnPO_4$ particle, carbon and finally flows into the Ni foil. During the discharge (reduction) process, Li^+ ion and electron follow the reverse route. Clearly, the slowest step involving Li^+ cation diffusion and/or electron transfer would be the rate determining step in the overall kinetics during the charge/discharge process. Compared with other doped samples, electrons and Li^+ cations easily diffuse through the Co-doped and V-doped $LiMnPO_4$ particles to its surface, and a relatively strong oxidation peak current is obtained as shown in Fig. 5.

By increasing the charging cut-off voltage to 4.8 V, there is 0.32–0.84 V differential between the charge and discharge plateau, bigger than those (0.23–0.54 V) at the cut-off voltage 4.4 V (as shown in Figs. 6 and 7). Moreover, there is a voltage differential (0.32–0.46 V) between the charge and discharge plateau for the Co-

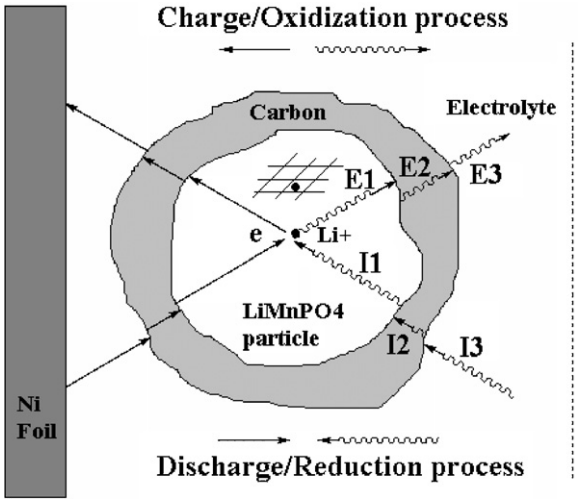

Fig. 12. The diffusion of Li^+ cation and the transfer of electrons through the $LiMnPO_4$ particles during the charge/discharge processes.

doped sample tested at 4.4, 4.6 and 4.8 V, respectively (as shown in Fig. 9). It indicates that the increased cut-off voltage cannot benefit for the diffusion ability of Li^+ cations.

By increasing testing temperature to 50 °C, there is 0.2–0.3 V differential between the charge and discharge plateau, greatly smaller than those (0.4–0.8 V) at the cut-off voltage 4.8 V and 25 °C (Fig. 8). It indicates that the increased testing temperature can greatly benefit for the diffusion ability of Li^+ cations during charging/discharging process. Because the lithium cation has similar diffusion ability in electrolyte at different cut-voltages and temperatures, the diffusion of lithium cation in the crystal lattice would be the important step during charging/discharging process.

4. Conclusion

Metal (alkali-, transition-, inner-transition-) ion doped, $LiMn_{0.95}M_{0.05}PO_4$ powders (M = Mg^{2+}, V^{3+}, Fe^{2+}, Co^{2+}, or Gd^{3+}) are synthesized by solid-state reaction route. The lattice parameters and crystal structure of those doped samples show little deviation to that of pure $LiMnPO_4$. The diffusion ability of Li^+ ions and the electrochemical performance of the cathode materials are shown to depend on the crystal structure. More precisely, the lengthening and weakening of the Li–O bonds are found to be conducive to the enhanced electrochemical performance of the synthesized doped products as cathode materials. The Li–O bonds of Co-doped and Gd-doped $LiMnPO_4$ samples are apparently lengthened leading to an enhanced electrochemical performance of these materials due to facile diffusion of Li^+ cation which in turn leads to better charging/discharging.

At the relatively higher testing temperature (50 °C), the Co-doped $LiMnPO_4$ sample showed the almost same discharge capacity, 151.9 and 149.3 mAh g^{-1} at 4.4 and 4.8 V, respectively. Moreover, there is 0.2–0.3 V differential value between the charging and discharging voltage plateau tested at 4.4 V and 50 °C, greatly smaller than those (0.4–0.8 V) at the cut-off voltage 4.8 V and 25 °C. It indicates that the increased testing temperature can greatly benefit for the diffusion ability of Li^+ cations during charging/discharging process. Overall electrochemical performance is an interesting interplay of lattice parameters, testing temperature, which in turn kinetically alters the Li-cation and electron availability in these materials. The study might provide helpful insights on the rationale of future design of $LiMnPO_4$ based high power lithium batteries with high charge/discharge capacities and with better cycle performance.

Acknowledgments

Gang Yang acknowledged the grant provided by Fundação para a Ciência e Tecnologia (Portugal) (SFRH/BPD/64217/2009). The work was supported by Natural Science Foundation of Jiangsu Province of China (Grant No. BK2010262), Natural Science Foundation of Jiangsu Educational Department of China (Grant No. 10KJA480001), and Natural Science Foundation of China (Grant No. 10874021).

References

[1] A.K. Padhi, K.S. Nanjundaswamy, J.B. Goodenough, J. Electrochem. Soc. 144 (1997) 1188.
[2] M.S. Islam, D.J. Driscoll, C.A.J. Fisher, P.R. Slater, Chem. Mater. 17 (2005) 5085.
[3] B. Kang, G. Ceder, Nature 458 (2009) 190.
[4] L. Wang, F. Zhou, G. Ceder, Electrochem. Solid-State Lett. 11 (2008) A94.
[5] G. Li, H. Azuma, M. Tohda, Electrochem. Solid-State Lett. 5 (2002) A135.
[6] H.S. Fang, Z.Y. Pan, L.P. Li, Y. Yang, G.F. Yan, G.S. Li, S.Q. Wei, Electrochem. Commun. 10 (2008) 1071.
[7] D.Y. Wang, H. Buqa, M. Crouzet, G. Deghenghi, T. Drezen, I. Exnar, N.-H. Kwon, J.H. Miners, L. Poletto, M. Grätzel, J. Power Sources 189 (2009) 624.
[8] Y.R. Wang, Y.F. Yang, Y.B. Yang, H.X. Shao, Solid State Commun. 150 (2010) 81.
[9] N.-H. Kwon, T. Drezen, I. Exnar, I. Teerlinck, M. Isono, M. Grätzel, Electrochem. Solid-State Lett. 9 (2006) A277.
[10] J. Molenda, W. Ojczyk, J. Marzec, J. Power Sources 174 (2007) 689.
[11] C. Delacourt, L. Laffont, R. Bouchet, C. Wurm, J.-B. Leriche, M. Morcrette, J.-M. Tarascon, C. Masquelier, J. Electrochem. Soc. 152 (2005) A913.
[12] D.Y. Wang, C.Y. Ouyang, T. Drézen, I. Exnar, A. Kay, N.-H. Kwon, P. Gouerec, J.H. Miners, M.K. Wang, M. Grätzel, J. Electrochem. Soc. 157 (2010) A225.
[13] A.V. Murugan, T. Muraliganth, P.J. Ferreira, A. Manthiram, Inorg. Chem. 48 (2009) 946.
[14] T. Drezen, N.-H. Kwon, P. Bowen, I. Teerlinck, M. Isono, I. Exnar, J. Power Sources 174 (2007) 949.
[15] R. Dominko, M. Bele, M. Gaberscek, M. Remskar, D. Hanzel, J.M. Goupil, S. Pejovnik, J. Jamnik, J. Power Sources 153 (2006) 274.
[16] C. Delacourt, P. Poizot, M. Morcrette, J.-M. Tarascon, C. Masqulier, Chem. Mater. 16 (2004) 93.
[17] T. Doi, S. Yatomi, T. Kida, S. Okada, J. Yamaki, Cryst. Growth Des. 9 (2009) 4990.
[18] Z. Bakenov, I. Taniguchi, Electrochem. Commun. 12 (2010) 75.
[19] Y. Zhang, C.S. Sun, Z. Zhou, Electrochem. Commun. 11 (2009) 1183.
[20] M. Kopec, A. Yamada, G. Kobayashi, S. Nishimura, R. Kanno, A. Mauger, F. Gendron, C.M. Julien, J. Power Sources 189 (2009) 1154.
[21] T. Shiratsuchi, S. Okada, T. Doi, J.-I. Yamaki, Electrochim. Acta 54 (2009) 3145.
[22] Z.X. Nie, C.Y. Ouyang, J.Z. Chen, Z.Y. Zhong, Y.L. Du, D.S. Liu, S.Q. Shi, M.S. Lei, Solid State Commun. 150 (2010) 40.
[23] A.C. Larson, R.B. Von Dreele, General Structure Analysis System (GSAS), Los Alamos National Laboratory Report LAUR (2000) 86-748.
[24] S.K. Martha, B. Markovsky, J. Grinblat, Y. Gofer, O. Haik, E. Zinigrad, D. Aurbach, T. Drezen, D. Wang, G. Deghenghi, I. Exnarb, J. Electrochem. Soc. 156 (2009) A541.
[25] M. Wagemaker, B.L. Ellis, D.L. Hecht, F.M. Mulder, L.F. Nazar, Chem. Mater. 20 (2008) 6313.
[26] A.V. Murugan, T. Muraliganth, A. Manthiram, J. Electrochem. Soc. 156 (2009) A79.